

Ductile to brittle fault zone evolution in Austroalpine units to the southeast of the Tauern Window (Eastern Alps)

Andreas Wölfler¹ · Wolfgang Frisch² · Harald Fritz³ · Martin Danišik⁴ · Anke Wölfler⁵

Received: 7 August 2014 / Accepted: 4 July 2015 / Published online: 28 July 2015
© Swiss Geological Society 2015

Abstract This study combines structural and thermochronological analysis with published geochronological data to evaluate the tectonic evolution of the ductile Main Mylonite Zone and the adjacent brittle Ragga–Teuchl fault to the southeast of the Tauern Window. The Main Mylonite Zone experienced ductile deformation with top-to-the-NW transport direction. From microstructural analysis and published K/Ar and Ar/Ar data the timing for this ductile deformation is proposed to be Late Cretaceous in age, contemporaneous to a well documented extensional collapse that affected large parts of the Eastern Alps. Subsequent brittle faulting affected the Main Mylonite Zone and neighbouring units. Apatite fission track data suggest that brittle deformation along the Ragga–Teuchl fault and adjacent units occurred in the middle- and late Miocene (~23 and ~11 Ma), contemporaneous with the main phase of lateral extrusion. Our results show that a rather small study area may comprise information about the evolution of the Eastern Alps from Late Cretaceous to late

Miocene times. We also demonstrate that low-temperature thermochronology is a viable tool to resolve the timing of brittle faulting and accompanied fluid activity.

Keywords Fault zones · Ductile deformation · Brittle deformation · Fission track dating · Eastern Alps

1 Introduction

Although the European Alps are investigated intensively by more than 200 years, there are still areas where modern data or even detailed geological maps are rare. One of these areas is situated in the Austroalpine units to the south-east of the Tauern Window, the so-called Kreuzeck Mountains (Figs. 1, 2a). In this area the WNW-trending, south-dipping Main Mylonite Zone (Hoke 1990) forms the contact between two units that differ significantly in their structural and metamorphic history (Figs. 2b, 3) (e.g. Schuster et al., 2004, 2013). Hoke (1990) already pointed out the importance of this shear zone that has been interpreted as a normal fault that was active from the Late Cretaceous to the Early Paleogene. In places the Main Mylonite Zone is affected by brittle faults, which rework the mylonites along their strike (Figs. 2b, 3).

The aim of this study is to shed more light into the kinematic and temporal evolution of the Main Mylonitic Zone and adjacent brittle faults. For this purpose we provide microstructural analysis of quartz-rich rocks including quartz texture analyses. Since it is well documented that both intracrystalline- and recovery processes are strongly T-dependent and form diagnostic microstructures and textures (e.g. Hirth and Tullis 1992; Stipp et al. 2002a, b, 2006) we will link our results with thermochronological data to evaluate the timing of deformation. To unravel the timing of brittle faulting we attempt to date thermal

Editorial handling: A. G. Milnes.

✉ Andreas Wölfler
woelfler@geowi.uni-hannover.de

¹ Institut für Geologie, Leibniz Universität Hannover, Callinstraße 30, 30167 Hannover, Germany

² Institut für Geowissenschaften, Wilhelmstraße 56, 72074 Tübingen, Germany

³ Institut für Erdwissenschaften, Karl-Franzens Universität Graz, 8010 Graz, Austria

⁴ Department of Earth and Ocean Sciences, Faculty of Science and Engineering, University of Waikato, Hillcrest Road, Hamilton, New Zealand

⁵ Department Angewandte Geowissenschaften und Geophysik, Montanuniversität Leoben, 8700 Leoben, Austria

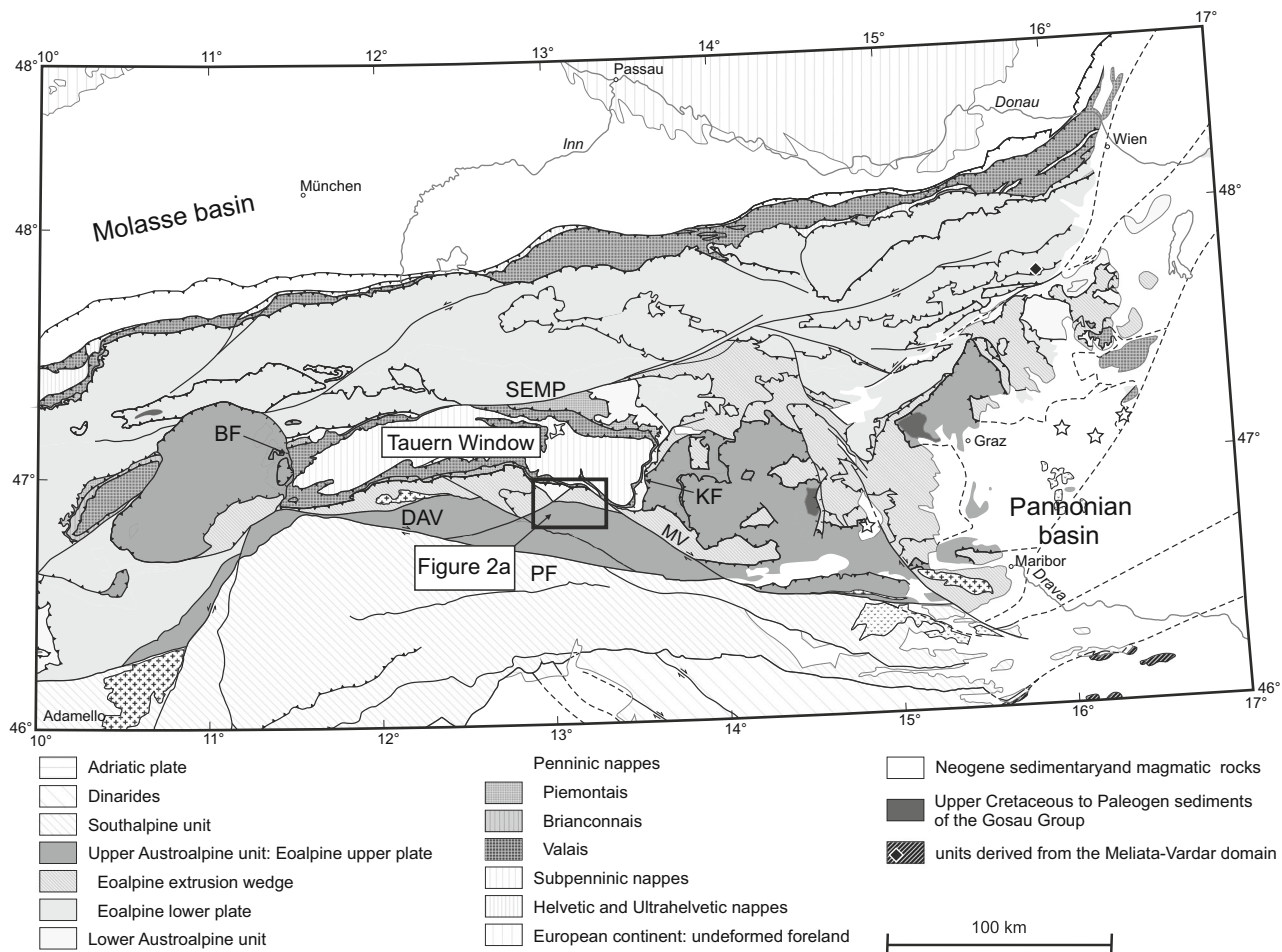


Fig. 1 Tectonic map of the Eastern Alps following the nomenclature of Schmid et al. (2004) (modified after Froitzheim et al. 2008). *BF* Brenner normal fault, *KF* Katschberg normal fault, *DAV* Deferegen-

Antholz-Vals fault, *SEMP* Salzach-Ennstal-Mariazell-Puchberg fault, *PF* Pustertal fault, *MV* Möll valley fault

anomalies within fault zones by comparison of zircon- and apatite fission track data (ZFT, AFT) at the transition from fault-related rocks to the undeformed host rock. For this we choose the Ragga–Teuchl fault, a cataclastic fault zone that borders the northern part of the Main Mylonite Zone in the east and strikes away from the mylonites in the western part of the study area (Fig. 2b, 3). Additionally we sampled a well exposed brittle fault to the north of the Ragga Teuchl fault (sample KR 5 in Fig. 2b). Our results show that multidisciplinary methods may provide information about the evolution of a rather small study area from the Late Cretaceous to Late Miocene times.

2 Geological setting and geochronology of the study area

The Eastern Alps are composed of units derived from the European continent, the Penninic oceanic realm and units derived from the Adriatic microplate (Figs. 1, 2a). The

Southalpine and Austroalpine units represent the Adriatic microplate and are widely exposed in the Eastern Alps while the units derived from the Penninic oceanic realm and the European margin are mainly exposed in tectonic windows like the Tauern Window (Fig. 1).

The study area is located to the southeast of the Tauern Window (Figs. 1, 2) which consist of polyetamorphic rocks which were overprinted from the Devonian to the Cretaceous (e.g. Hoinkes et al. 1999; Neubauer et al. 1999). The WNW-trending, south-dipping Main Mylonite Zone is situated at the contact of the Prijakt–Polinik and Strieden Complex to the north and south, respectively (Fig. 2) (Schuster et al. 2004, 2013). The mylonitic foliation and stretching lineation generally strikes E–W and/or WNW–ESE (Fig. 3) and kinematic indicators suggest that the Main Mylonite Zone acted as a normal fault where the Strieden Complex moved over the Prijakt–Polinik Complex (Hoke 1990).

The Prijakt–Polinik Complex experienced a metamorphic imprint under amphibolite to eclogite facies conditions during the Eo-Alpine metamorphism (Schmid et al. 2004;

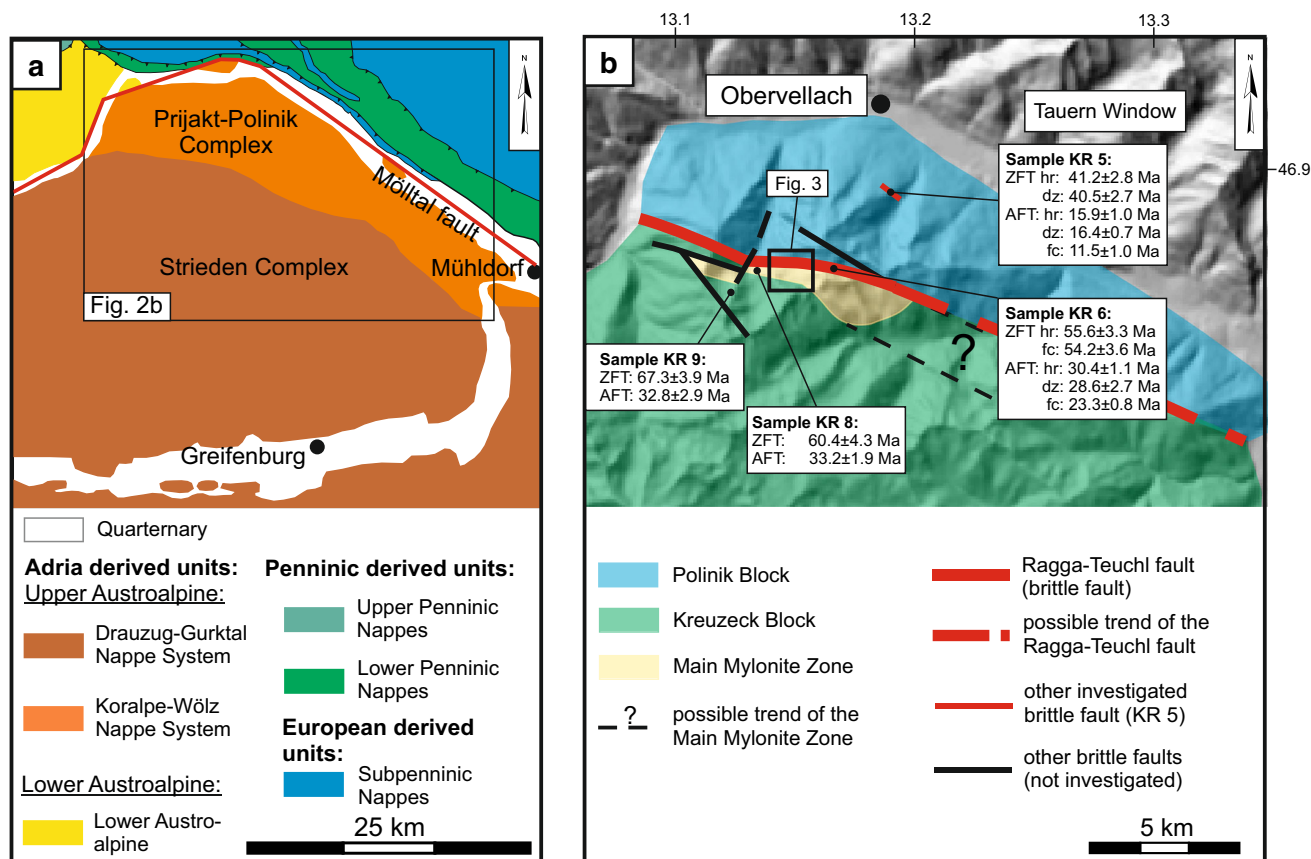


Fig. 2 **a** Tectonic map of the Kreuzeck Mountains and neighbouring areas (modified after Schuster et al. 2013). **b** Digital elevation model of the study area with sample localities of fission track samples (coordinates are given in Tables 1 and 2)

Schuster et al. 2001, 2004). Published geochronological data from the Prijakt-Polinik Complex include Cretaceous K/Ar- and Ar/Ar ages on white mica and biotite (Oxburgh et al. 1966; Lambert 1970; Waters 1976; Hoke 1990; Dekant 2009; Wölfler et al. 2015). The Strieden Complex experienced only an anchizonal to lowermost greenschist facies Eo-Alpine imprint (Schuster et al. 2001, 2004). K/Ar and Ar/Ar ages on white mica and biotite reported from the Strieden Complex are between 337 and 141 Ma (Brewer and Jenkins 1969; Brewer 1970; Waters 1976; Hoke 1990; Dekant 2009; Wölfler et al. 2015).

During the Miocene lateral extrusion the whole area was affected by steeply dipping brittle faults (Figs. 2b, 3). According to the distribution of ZFT and AFT data, the Ragga-Teuchl fault separates the study area into two domains with different ages (Wölfler et al. 2008). The Polinik Block to the north of the Ragga-Teuchl (Fig. 2b) fault displays ZFT and AFT data from 45 to 30 Ma and 23 to 7 Ma, respectively (Staufenberg 1987; Dunkl et al. 2003; Wölfler et al. 2008, 2015). The southern block, referred to as Kreuzeck Block (Fig. 2b), is characterised by ZFT and AFT ages from 160 to 54 Ma (Dunkl et al. 2003;

Wölfler et al. 2008, 2015) and 33 to 20 Ma (Staufenberg 1987; Wölfler et al. 2008, 2015), respectively. Since the Main Mylonite Zone and the Ragga-Teuchl fault were active at different times we refer the terms Prijakt-Polinik and Strieden Complex to the Cretaceous to Paleogene activity of the Main Mylonite Zone and the terms Polinik and Kreuzeck Blocks to the Oligocene to Miocene activity of the Ragga-Teuchl fault.

3 Methods

The study of microstructures and textures of quartz is aimed to document possible changes in deformation mechanisms that are known to be sensitive to temperature, strain rate, stress and water content (e.g. Hirth and Tullis 1992; Stipp et al. 2002a, b, 2006). For temperature estimates of different dynamic recrystallization mechanisms of quartz we refer to Stipp et al. (2002a). Therefore, below ~300 °C pressure solution and cataclasis are the main deformation mechanisms. Bulging mechanisms (BLG) are active between ~300 and 400 °C and subgrain rotation

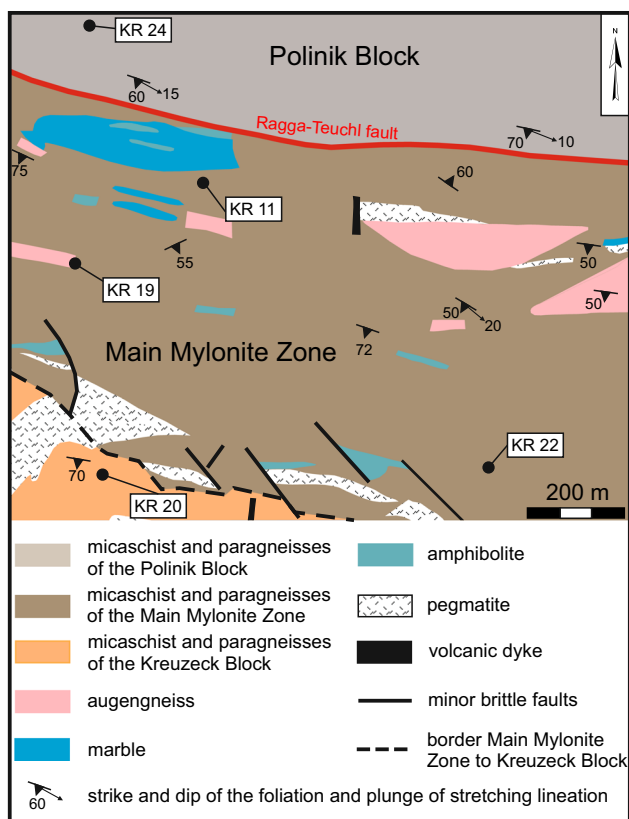


Fig. 3 Simplified geological map of the study area (modified after Hoke 1990) with localities of CPO samples. Coordinates (WGS 1984) and elevation: KR 11: N 46°53'27.6" E 13°08'20.4" 1924 m; KR 19: N 46°53'13.2"E 13°08'9.6" 2080 m; KR 20: N 46°53'06" E 13°53'06.12" 2230 m; KR 22: N 46°53'02.4" E 13°08'49.2" 2220 m; KR 24: N 46°53'34.8" E 13°08'16.8" 1872 m

mechanisms (SGR) are dominant between ~ 400 and 500 °C. At temperatures above ~ 500 °C grain boundary migration recrystallization (GBM) is dominant.

We used the X-ray texture goniometer facility of the Institute of Earth Sciences, University Graz in Austria to evaluate crystallographic preferred orientation of quartz. Polished rock chips were placed in the X-ray beam of a texture goniometer (wavelength $\text{CuK}\alpha = 1.5418$, beam current = 40 kV and 40 mA) used in reflection mode. The Bruker Analytical Systems X-ray texture goniometer (D8 Discover) is equipped with an area detector (Gadds HTS). Eight lattice directions ($\langle 100 \rangle$, $\langle 110 \rangle$, $\langle 102 \rangle$, $\langle 200 \rangle$, $\langle 201 \rangle$, $\langle 112 \rangle$, $\langle 211 \rangle$, $\langle 113 \rangle$) have been measured at angle between 0° (center) and 80° (periphery). Fourier analysis were applied for correction of defocusing effects. Lattice planes $\langle 001 \rangle$, $\langle 101 \rangle$ and $\langle 011 \rangle$ were calculated using the orientation density function (ODF) based on the harmonic method of Roe (1965) and Bunge (1981). For detailed description of the technical procedure see Wenk (1985). Representative $\langle c \rangle$ -axes ($\langle 001 \rangle$) and a-axes

($\langle 110 \rangle$) orientation distributions are shown as pole figures. In all diagrams the foliation is vertical E–W and the stretching lineation X is oriented horizontal E–W, Y is the centre and Z, the direction of minimum extension is N–S. From the asymmetry of $\langle c \rangle$ -axes and a-axes with respect to the foliation, the sense of shear was determined.

For fission track thermochronology we used the zircon- and apatite fission track (ZFT, AFT) methods, whose sensitivity intervals are referred to as zircon- and apatite fission track partial annealing zones (ZPAZ, APAZ), ranging from 300 to 200 °C and 120 to 60 °C, respectively (Wagner and Van den haute 1992; Green et al. 1986). The zeta calibration approach was used to determine the ages (Hurford and Green 1983). For thermal history modelling of ZFT and AFT data we used the HeFTy software (Ketcham 2005) with annealing algorithm of Ketcham et al. (1999). We used the following input parameters: single grain AFT ages, c-axis corrected track lengths with standard deviation, Dpar values as kinetic parameters (Dpar: mean diameter of etch figures on prismatic surfaces of apatites parallel to the crystallographic c-axis; Burtner et al. 1994). The starting conditions of the samples are constrained by the ZFT ages and their one sigma errors within the temperature range of 300 – 200 °C. Final modelling constraint is the surface temperature of ~ 10 °C.

For dating thermal anomalies within brittle fault zones we sampled two sites with well exposed fault cores, damage zones and host rocks (Figs. 2b, 4). The first one is situated in the Polinik Block (sample KR 5 in Fig. 2b) and displays a ~ 1 m wide fault core that is surrounded by a ~ 5 m wide damage zone (Fig. 4a, d). The fault core consists of a fine grained gouge- and cataclasite matrix with clasts that partly reach ~ 50 μm in diameter (Fig. 4b) and the damage zone is characterized by a strongly fractured gneiss (Fig. 4c). The second brittle fault zone is situated along the Ragga–Teuchl fault and consist of a ~ 5 m wide fractured zone with several fault cores that is surrounded by a ~ 10 m wide damage zone (Fig. 4e). In the area of investigation the brittle fault plane dips steeply to the south ($185/80$). In contrast to the single fault core of the fault zone in the Polinik Block (Fig. 4a, d), the fault core consists of several branching and anastomosing cores that are separated by a strongly fractured damage zone material (Fig. 4e). The damage zone is composed of a strongly sheared orthogneiss. The fault core related rocks continuously develop from fault breccias and coarse grained cataclasites towards fine-grained cataclasites and fault gouges. Both, fault cores and damage zones display signatures of faulting and/or fluid circulation, such as the occurrence of cataclasites and fault gouges, slickensides and secondary grown minerals.

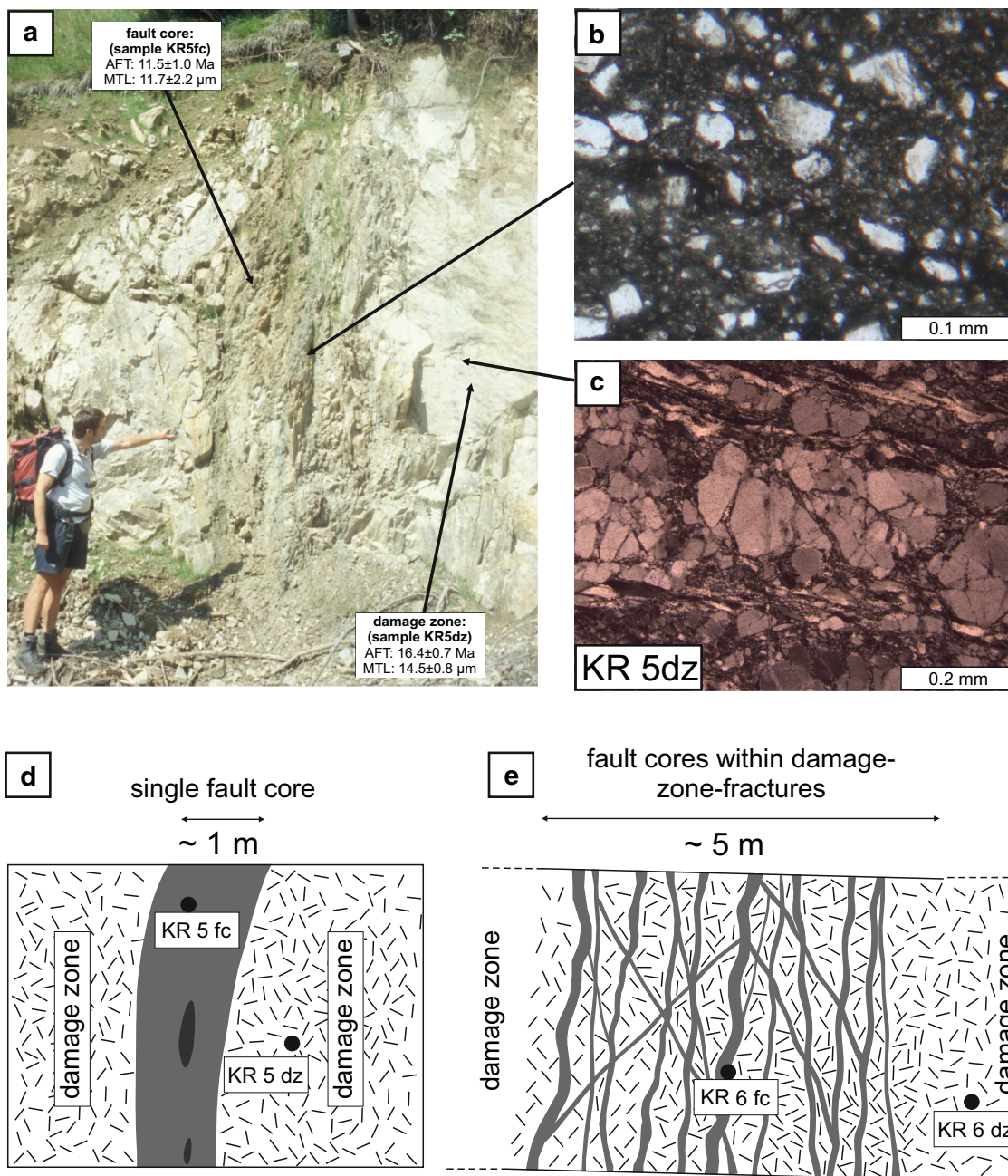


Fig. 4 a Damage zone and fault core (sample KR5) within the Polinik Block. AFT ages and track length distributions differ significantly (orientation of the fault plane: 045/79). b Fine grained gouge material of the brittle fault. c Damage zone structure of the brittle fault. d Sketch of the brittle fault in the Polinik Block. The fault zone comprises on single fault core composed fine-grained, grey-coloured gouges and lensoid dark cataclasites (shown in black). KR5

fc (fault core) and KR5 dz (damage zone) display sample localities for fission track analysis. For comparison see Fig. 4a. e Sketch of the brittle structure along the Ragga–Teuchl fault. The fault zone shows multiple cores that are separated and surrounded by damage zone material. KR6 fc (fault core) and KR6 dz (damage zone) display sample localities for fission track analysis

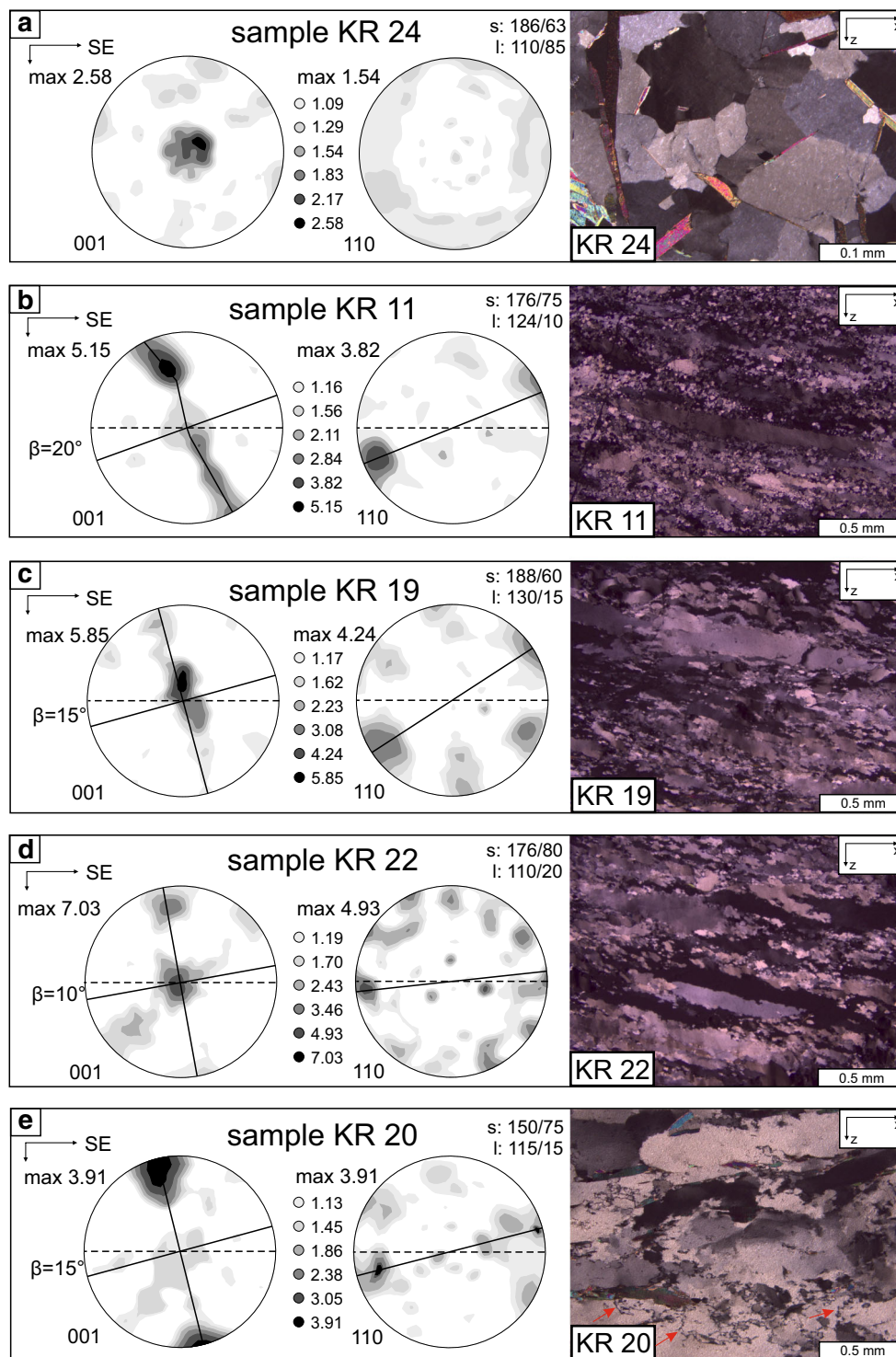


Fig. 5 CPO and Quartz microstructures from the (a) Prijakt–Polinik Complex, the Main Mylonite Zone (b, c and d) and from the Strieden Complex (e). The red arrows in (e) document microcracks. The pole

figures are lower hemisphere projections nad logarithmic graduated. Schistosity (s) and lineation (l) are given in the top right corner of the pole figures

Fig. 6 Zircon- (ZFT), apatite fission track (AFT) ages and mean track length distributions (MTL) against elevation for the Kreuzeck Block, the Polinik fault and the Polinik Block. *Circles* Kreuzeck Block; *squares* Polinik fault; *polygons* Polinik Block; *black* host rock (hr); *green* damage zone (dz); *red* fault core (fc)

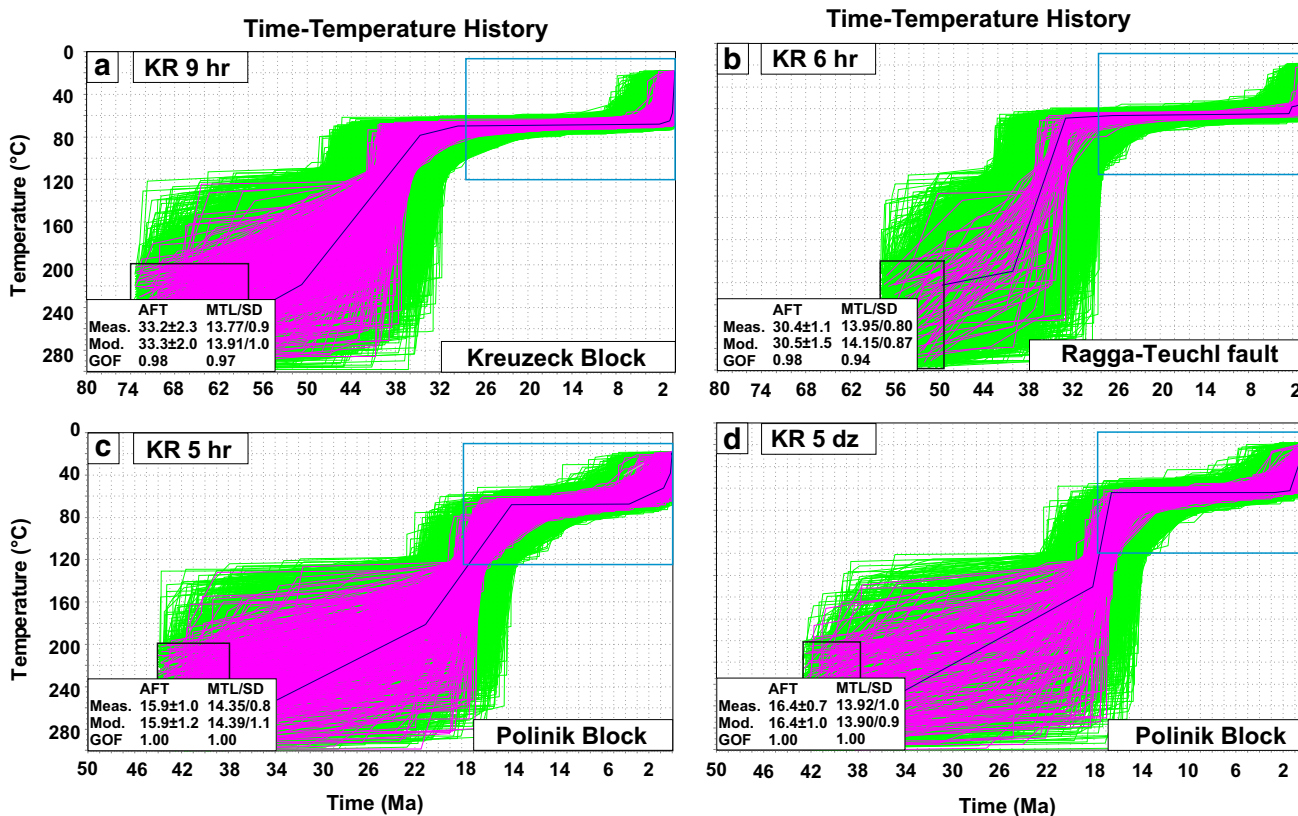
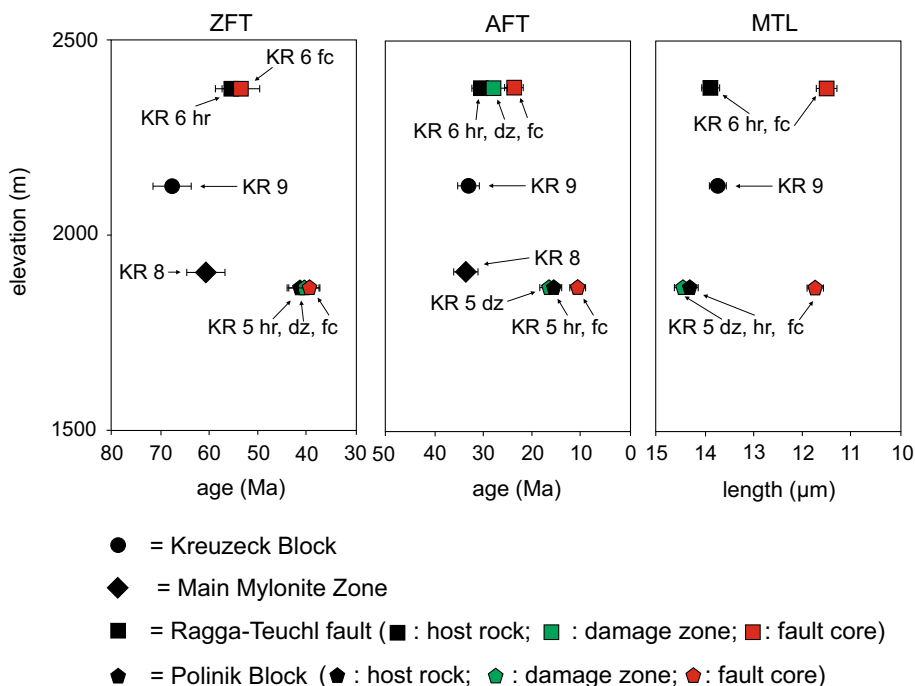


Fig. 7 Thermal history inverse models using the HeFTy program (Ketcham 2005). Input parameters: central AFT age with 1 σ error, track length distributions, Dpar values as kinematic parameters. *Meas.* measured age, *Mod.* modeled age, *GOF* goodness of fit, *AFT* apatite

fission track age, *MTL/SD* mean track length/standard deviation. *Black boxes* are starting conditions defined by the corresponding ZFT ages; *blue boxes* define final cooling; *green paths* acceptable fit; *red paths* good fit; *black line* best fit

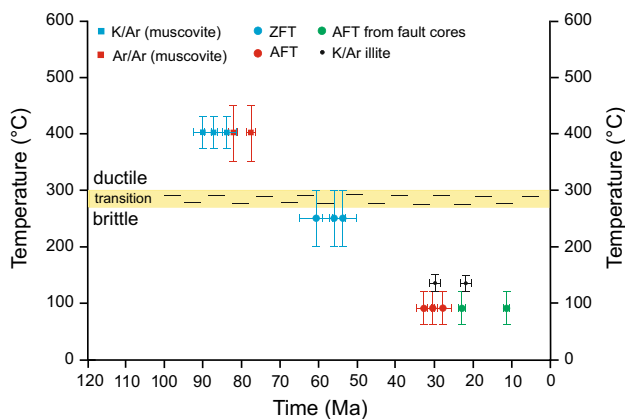


Fig. 8 Summary of geo- and thermochronological data from the Main Mylonite Zone. K/Ar (muscovite): Waters (1976), Hoke (1990); Ar/Ar (muscovite): Dekant (2009); ZFT: this study; AFT: this study; K/Ar (illite): Kralik et al. (1987)

4 Results

4.1 Quartz microstructures and crystallographic preferred orientations (CPO)

The quartz microstructures from the Polinik Block (sample KR24 of Fig. 3) are characterized by polygonal quartz grains with mainly straight boundaries partly showing 120° triple junctions and a grain size of up to 0.5 mm (Fig. 5a). The CPO pole figures of this sample display c-axes [001] and a-axes [110] with a tendency towards the formation of a single girdle distribution (Fig. 5a). The maximum of the c-axes is located at the Y-axis of the finite strain ellipsoid and the a-axes are symmetrically arranged with respect to the foliation (Fig. 5a).

The quartz microstructures from the Main Mylonite zone (samples KR11, KR19, KR22 of Fig. 3) display sutured grain boundaries and elongated porphyroclasts forming ribbon grains (Figs. 5b, c, d) with a long axis of up to 1 mm. Recrystallized grains are small and do not exceed 0.03 mm. In places the formation of core-mantle structures can be observed (Fig. 5b). The grain boundaries are largely irregular and undulatory extinction and bulges are widespread features.

The CPO pole figures of sample KR11 displays a single girdle distribution with one peripheral maximum oblique to Z (Fig. 5b). The asymmetry of the c-axes indicates a top-to-the-NW shear component. The a-axes are accordingly distributed along a great circle which is 20° oblique to the trace of the foliation, thus confirming a top-to-the-NW displacement (Fig. 5b). The c-axes distribution of sample KR19 shows a main maximum close to Y with a relict or weak single girdle distribution (Fig. 5c). The asymmetry of the c-axes distributions is 15° oblique to the foliation and documents a top-to-the-NW shear component (Fig. 5c).

Two a-axes maxima are symmetrically distributed around the lineation with an opening angle of 15°. The unequal maxima indicate a transition from single to type I cross girdle with stronger maximum pointing towards sinistral, i.e. top NW shearing (Fig. 5c). Samples KR22 and KR20 show c- and a-axes indicating a mixed single-cross girdle distribution which indicates a combination of pure and simple shear (Figs. 5d, e). Sample KR20 from the Kreuzeck Block shows large quartz porphyroclasts that appear only slightly elongated (Fig. 5e). Widespread features are undulose and patchy extinction, bulges and microcracks (arrows in Fig. 5e). Bulges are developed along grain boundaries and along fractures. The main deformation mechanism is bulging recrystallization. The c-axes and a-axes distributions are characterized by a single girdle distribution that is 15° oblique to the foliation, documenting top-to-the-NW transport (Fig. 5d).

4.2 Fission track data and thermal history models

ZFT and AFT ages are reported as central ages with 1 sigma errors and are summarized in Tables 1 and 2. Sample locations and age data are indicated in Fig. 2b and Tables 1 and 2. Samples KR5 and KR6 are from brittle faults and each comprise one sample from the fault core (KR5 fc, KR6 fc) one from the damage zone (KR5 dz, KR6 dz) and one from the host rock (KR5 hr, KR6 hr). That means that for these two samples three different rocks have been sampled which have the same capital letters and numbers.

Sample KR9 from the Kreuzeck Block displays ZFT and AFT ages of 67.3 ± 3.9 Ma and 32.8 ± 2.9 Ma, respectively (Figs. 2b, 6 Tables 1, 2). Sample KR8 from the Main Mylonite Zone has a ZFT age of 60.4 ± 4.3 Ma and an AFT age of 33.2 ± 1.9 Ma. The samples KR6 hr and KR6 fc from the Ragga-Teuchl fault display ZFT ages of 55.6 ± 3.3 and 54.2 ± 3.6 Ma, respectively. The AFT ages of the samples KR6 hr and KR6 dz overlap within 1 sigma error and are characterized by similar track length distributions (KR6 hr: 30.4 ± 1.1 Ma and 13.95 ± 0.8 μm ; KR6 dz: 28.6 ± 2.7 Ma and 13.51 ± 1.26 μm). However, the fault core sample KR6 fc displays a younger AFT age and shorter track lengths (23.3 ± 0.8 Ma and 11.51 ± 1.95 μm) (Figs. 2b, 6; Table 2).

The same applies to the samples from the brittle fault zone in the Polinik Block (sample KR5). The host rock sample yields a ZFT and AFT age of 41.2 ± 2.8 and 15.9 ± 1.0 Ma, respectively. The samples from the damage zone display a ZFT age of 40.5 ± 2.8 and a AFT age of 16.4 ± 0.7 . Although the ZFT age from the fault core sample of 40.1 ± 2.2 is similar compared to the ages from the damage zone and host rock (Figs. 2b, 6; Table 1) the

Table 1 New zircon fission track data

Sample code	Long.	Lat.	Elevation (m.a.s.l.)	<i>n</i>	ρ_s	ρ_i	N_s	N_i	ρ_d	N_d	$P(\chi^2)$ (%)	Age (Ma)	$\pm 1\sigma$ (Ma)
KR 9	13°07'01"	46°52'56"	2130	20	101.722	958	64,028	603	6886	3089	99.2	67.3	3.9
KR 8	13°07'32"	46°53'19"	1714	20	101.460	922	64,502	598	6812	3089	93.2	60.4	4.3
KR 6 hr	13°09'45"	46°53'17"	2380	20	100.929	980	64,982	623	6901	3089	92.8	55.6	3.3
KR 6 fc	13°09'45"	46°53'17"	2380	20	101.098	989	64,835	600	6851	3089	98.4	54.2	3.6
KR 5 hr	13°10'57"	46°54'29"	1883	20	99.897	790	63,291	572	6734	3089	99.3	41.2	2.8
KR 5 dz	13°10'58"	46°54'28"	1870	20	100.012	809	63,498	604	6733	3089	94.5	40.5	2.8
KR 5 fc	13°10'58"	46°54'28"	1870	20	100.047	901	64,281	650	6629	3089	97.3	40.1	2.2

n, Number of dated apatite crystals; ρ_s/ρ_i , spontaneous/induced track densities ($\times 10^5$ tracks/cm²); N_s/N_i , number of counted spontaneous/induced tracks; ρ_d , dosimeter track density ($\times 10^5$ tracks cm²); N_d , number of tracks counted on dosimeter; $P(\chi^2)$, probability obtaining Chi square (χ^2) value for *n* degrees of freedom (where *n* is number of crystals minus 1); age $\pm 1\sigma$ is central age ± 1 standard error (Galbraith and Laslett 1993); ages were calculated using zeta calibration method (Hurford and Green 1983); glass dosimeter CN-2; hr, host rock; dz, damage zone; fc, fault core

AFT data from the fault core display younger AFT ages and shorter MTL (11.5 Ma and 11.75 μ m) as observed in the corresponding damage zone and host rock (Figs. 2b, 6; Table 2).

Both fault core samples display not only shorter MTL but also a bimodal distribution of the track lengths and a large standard deviation (Table 2) that are typical for reheated samples (Gleadow et al. 1986).

The thermal history models of host rock samples KR9 hr, and KR6 hr demonstrate that the Kreuzeck Block and the samples from the Ragga-Teuchl fault entered the APAZ in Eocene/Oligocene times (Fig. 7a, b). In contrast, the Polinik Block reached the temperature range of the APAZ in the early Miocene (Sample KR 5 hr and KR5 dz in Fig. 7c, d).

5 Interpretation and discussion

5.1 Deformation mechanisms and kinematics related to the regional geological frame

Quartz microstructures from the Main Mylonite Zone are characterized by bulging, sutured grain boundaries, undulatory extinction and a size of recrystallized grains that do not exceed 0.03 mm. These features are indicative for bulging recrystallization (Stipp et al. 2002a, 2010). In places, the formation of core-mantle structures document the transition from bulging recrystallization to subgrain rotation recrystallization (Stipp et al. 2002a). Both recrystallization mechanisms are dominant at temperatures between ~ 300 and ~ 450 °C, thus at greenschist facies conditions (Stipp et al. 2002a, 2004).

The temperature range for the muscovite K/Ar and Ar/Ar systems are 430–375 °C and 450–350 °C, respectively

(Hames and Bowering 1994; Kirschner et al. 1996; Lips et al. 1998; Harrison et al. 2009), and are in the same range as the temperatures for bulging recrystallization. K/Ar and Ar/Ar muscovite data from the Main Mylonite Zone are between 90 and 78 Ma (Brewer and Jenkins 1969; Brewer 1970; Hoke 1990; Dekant 2009; Wölfler et al. 2015).

As the CPO data indicate top-to-the-NW directed shearing (Figs. 5b–d), we propose that this deformation occurred in the Late Cretaceous contemporaneous to a phase of extension that has been observed in different parts of the Austroalpine nappe stack (e.g. Froitzheim et al. 1997, 2012; Fügenschuh et al. 2000; Liu et al. 2001; Kurz and Fritz 2003). Substantial parts of the Austroalpine nappe pile was overprinted by normal faulting during the Late Cretaceous, associated with formation of the Gosau sedimentary basins (Wagreich 1995; Froitzheim et al. 1994; Neubauer et al. 1995, 2000). In this context the Main Mylonite Zone acted as a normal fault (Hoke 1990) that brought the Strieden Complex on top of the Prijakt–Polinik Complex.

As the transition from ductile to semi-brittle and brittle deformation has been determined between ~ 300 and ~ 270 °C (Handy et al. 1999; Stipp et al. 2002a) and the temperature range of the ZFT system ranges between 300 and 200 °C (Wagner and van den Haute 1992), the ZFT data from the Main Mylonite Zone of 60.4 ± 4.3 (Fig. 2b) is considered as the lowermost age limit for ductile to semi-brittle deformation. Since then the Main Mylonite Zone resided in the brittle part of the upper crust (Fig. 8).

Metamorphic conditions in the Polinik Complex reached peak temperatures of 620 °C at ~ 100 Ma (Hoke 1990). Available Ar/Ar and ZFT ages range from 101 to 67 Ma and 45–30 Ma, respectively (Hoke 1990; Dekant 2009; Wölfler et al. 2008, 2015). The observed quartz microstructures from the Polinik Complex differ from

Table 2 New apatite fission track data

Sample code	Long.	Lat.	Elevation (m. a.s.l.)	n	ps	Ns	pi	Ni	pd	Nd	$P(\chi^2)$ (%)	Age (Ma)	$\pm 1\sigma$ (Ma)	MTL (μm)	SD (μm)	N (L)	Dpar (μm)
KR 9	13°07'01"	46°52'56"	2130	25	2.201	233	4134	1032	8049	15,118	99.2	33.2	2.9	13.77	0.89	55	2.06
KR 6 h	13°09'45"	46°53'17"	2380	25	2.221	245	4151	1080	7099	15,118	98.1	30.4	1.1	13.95	0.80	56	1.78
KR 6 dz	13°09'45"	46°53'17"	2380	25	2.139	240	4190	1038	7128	15,118	98.4	28.6	2.7	13.51	1.26	60	1.87
KR 6 fc	13°09'45"	46°53'17"	2380	25	1.277	303	6105	1450	7044	12,503	96.1	23.3	0.8	11.51	1.95	67	1.83
KR 5 h	13°10'57"	46°54'29"	1883	25	1.655	166	4120	1089	7207	15,118	99.9	15.9	1.0	14.35	0.81	70	1.87
KR 5 dz	13°10'58"	46°54'28"	1870	25	1.291	220	4087	1022	8054	15,118	89.8	16.4	0.7	13.92	1.02	54	2.01
KR 5 fc	13°10'58"	46°54'28"	1870	25	1.722	177	4640	1132	4509	15,118	93.3	11.5	1.0	11.75	2.11	68	1.93

n, Number of dated apatite crystals; ρ_s/ρ_i , spontaneous/induced track densities ($\times 10^5$ tracks/cm²); N_s/N_i , number of counted spontaneous/induced tracks; ρ_d , dosimeter track density ($\times 10^5$ tracks/cm²); Nd: number of tracks counted on dosimeter; $P(\chi^2)$, probability obtaining Chi square value (χ^2) for n degree of freedom (where n is number of crystals minus 1); MTL, mean track length; SD, standard deviation of track length distribution; N(L), number of horizontal confined tracks measured; Dpar, average etch pit diameter of fission tracks; age $\pm 1\sigma$ is central age ± 1 standard error (Galbraith and Laslett 1993); ages were calculated using zeta calibration method (Hurford and Green 1983); glass dosimeter CN-5

those of the Main Mylonite Zone. They are characterized by polygonal grains with straight grain boundaries, partly forming triple junctions (Fig. 5a). This is indicative for static recrystallization at amphibolites facies conditions at least at $\sim 500^\circ$ (e.g. Stipp et al. 2002a). We therefore suggest that static recrystallization occurred after metamorphic peak conditions in the Late Cretaceous.

Quartz microstructures from the Strieden Complex are dominated by bulging recrystallization that demonstrate deformation at lower temperatures, roughly between 300 and 400 °C (Stipp et al. 2002a) (Fig. 7e). The CPO data show an asymmetry of the pole figure that indicates top-to-the-NW directed deformation too (Fig. 5e). The Strieden Complex displays Ar/Ar and K/Ar data of white mica that are between 226 and 141 Ma (Hoke 1990; Dekant 2009; Wölfler et al. 2015) and ZFT ages range from 160 to 60 Ma (Dunkl et al. 2003; Wölfler et al. 2008, 2015). Due to this large spread in age data we are not able to estimate the age of the NW-directed deformation in the Strieden Complex. However, we speculate that it is also related to the late Cretaceous NW-directed deformation as observed in the Main Mylonite Zone, just a few meters away (Fig. 3) and as also observed by Hoke (1990).

In summary we conclude that the observed deformation along the Main Mylonite Zone is related to the well documented late Cretaceous extensional phase in the Eastern Alps.

5.2 Fission track data and implications for brittle deformation

The distribution of fission track data and the modelled thermal histories demonstrate that the Kreuzeck and Polinik Block experienced different cooling histories during the Paleogene and Neogene (Fig. 7). Cooling to conditions of the APAZ occurred during Oligocene/early Miocene and middle Miocene times for the Kreuzeck and Polinik Block, respectively. This difference has already been interpreted as a consequence of extension during Miocene lateral extrusion (Wölfler et al. 2008). Therefore the Ragga–Teuchl fault marks the border between foot-wall and hanging wall units (Polinik- and Kreuzeck Block, respectively) that experienced different cooling histories between the Oligocene and middle Miocene (Wölfler et al. 2015).

The sampled brittle fault zones display different widths and architecture of the corresponding fault core (Fig. 4d, e). Additionally, both fault cores are situated in different host rocks i.e. a paragneiss in the the fault zone in the Polinik Block (sample KR 5 in Figs. 2b, 4a, d) and an orthogneiss in the sample of the Ragga-Teuchl fault (sample KR 6 in Figs. 2b, 4e). Therefore, the different style of the fault cores may reflect differences in

mechanical strength between host rock and fault zone (e.g. Faulkner et al. 2010).

The ZFT ages of fault related rocks of the Ragga–Teuchl fault and the Polinik Block are similar to those of the host rocks (Figs. 2b, 6). However, fault core related AFT ages are younger and corresponding track lengths are shorter than in the related damage zones and fault cores (Figs. 2b, 6). By applying ZFT, AFT and apatite (U-Th)/He dating, several studies demonstrated significant thermal anomalies due to the infiltration of hot fluids in brittle faults (Tagami et al. 2001; Tagami and Murakami 2007; Yamada et al. 2007; Wölfler et al. 2010, Kurz et al. 2011; Emmel et al. 2012). However, dating of frictional heating was not successful so far (e.g. d’Alessio et al. 2003; Tagami 2012 and references therein). The main reason is possibly related to the short distances over which heat is generated along a fault zone. For a single earthquake, the most significant temperature increase is confined to a ~10-cm-wide zone of the slip surface, and temperature typically returns to a level similar to the pre-earthquake level after a few days (d’Alessio et al. 2003). Although the presence of pseudotachylites has been documented along the Ragga–Teuchl fault (Hoke 1990) it is not clear if frictional heating, fluid flow or possibly a combination of both was responsible to shorten track lengths and to rejuvenate AFT ages. Temperatures during pseudotachylite formation are expected to exceed ~1300 °C (e.g. Toyoshima 1990; Otsuki et al. 2003). Accordingly we would expect an impact on the ZFT system too. However, the ZFT system of the fault related rocks is not affected by secondary heating. A possible explanation is that fault cores may act as a short-lived, syndeformational fluid flow conduit that rapidly seals to form a barrier to flow (Caine et al. 1996). In that case, fluid flow occurred during, or shortly after brittle deformation. Therefore the AFT ages of the fault cores provide indirect information on the timing of brittle faulting, thus at ~23 ± 0.8 Ma, along the Ragga–Teuchl fault and ~11.5 ± 1.0 Ma along the brittle fault in the Polinik Block (Fig. 2b). The inferred timing of brittle faulting and accompanied fluid infiltration at ~23 Ma fits with K/Ar data of fault gouges from the Ragga–Teuchl fault (~23 Ma, Kralik et al. 1987) and faulting at ~11 Ma may correspond to brittle faulting in the Penninic units immediately to the north of the study area (Wölfler et al. 2008, 2012). Additionally the data correspond to the main phase of lateral extrusion between ~23 and 12 Ma (e.g. Frisch et al. 1998, 2000, Wölfler et al. 2011).

In summary, we present two arguments in favour of brittle deformation along the sampled fault zones in early and late Miocene times. (1) The fault core samples display significantly reduced mean track lengths with a bimodal distribution and younger AFT ages as compared to those of the host rocks or damage zones. (2) The inferred timing of

the assumed brittle faulting corresponds to already published data of brittle fault movement along the Ragga–Teuchl fault or in its immediate neighborhood (Kralik et al. 1987; Wölfler et al. 2008, 2012).

6 Conclusions

Structural and thermochronological investigations from the ductile Main Mylonite Zone and the brittle Ragga–Teuchl fault to the southeast of the Tauern Window document the evolution from Late Cretaceous to late Miocene times. Ductile deformation along the Main Mylonite Zone occurred under greenschist facies conditions in the Late Cretaceous. The structural analysis document top-to-the-NW directed deformation that goes along with the general extensional phase during the Late Cretaceous. Thermochronological analysis of fault related rocks suggest a thermal imprint in the early- and late Miocene that is possibly related to fluid circulation during or shortly after faulting.

Acknowledgments The thoughtful and constructive comments by Ralf Schuster and Bernhard Fügenschuh greatly improved the manuscript. We also would like to thank our editor Stefan Schmid for considerate handling of the manuscript and helpful comments. We thank Andrea Hampel and Christoph Glotzbach for constructive discussions and a review of an earlier version of the manuscript. This study was supported by the German Science Foundation (DFG-project FR 610/22).

References

- Brewer, M. (1970). K–Ar age studies in the Eastern Alps: The Oberostalpindecke of Kärnten. PhD Thesis, University of Oxford.
- Brewer, M., & Jenkins, H. (1969). Excess radiogenic argon in metamorphic micas from the Eastern Alps, Austria. *Earth and Planetary Science Letters*, 6, 321–331.
- Bunge, H. J. (1981). Fabric analysis by orientation distribution functions. *Tectonophysics*, 78, 1–21.
- Burtner, R. L., Nigrini, A., & Donelick, R. A. (1994). Thermochronology of Lower Cretaceous source rocks in the Idaho–Wyoming thrust belts. *AAPG Bulletin*, 78, 1613–1636.
- Caine, J. S., Evans, J. P., & Forster, C. B. (1996). Fault zone architecture and permeability structure. *Geology*, 24, 1025–1028.
- d’Alessio, M. A., Blythe, A., & Bürgmann, R. (2003). No frictional heat along the San Gabriel fault, California: Evidence from fission-track thermochronology. *Geology*, 31, 541–544.
- Dekant, C. (2009). Investigations on the magmatic and metamorphic history of the Kreuzeck Massif, Carinthia, Austria. *Tübinger Geowissenschaftliche Arbeiten, Reihe A*, 75, 68.
- Dunkl, I., Frisch, W., & Grundmann, G. (2003). Zircon Fission track thermochronology of the southeastern part of the Tauern Window and the adjacent Austroalpine margin, Eastern Alps. *Eclogae Geologicae Helvetiae*, 96, 209–217.
- Emmel, B., Lisker, F., & Hewawasam, T. (2012). Thermochronological dating of brittle structures in basement rocks: A case study from the onshore passive margin of SW Sri Lanka. *Journal of Geophysical Research*. doi:10.1029/2012JB009136.

- Faulkner, D. R., Jackson, C. A. L., Lunn, R. J., Schlische, R. W., Shipton, Z. K., Wibberly, C. A. J., & Withjack, M. O. (2010). A review of recent developments concerning the structure, mechanics and fluid flow properties of fault zones. *Journal of Structural Geology*, *32*, 1557–1575.
- Frisch, W., Dunkl, I., & Kuhleman, J. (2000). Post-collisional orogen-parallel large-scale extension in the Eastern Alps. *Tectonophysics*, *327*, 239–265.
- Frisch, W., Kuhleman, J., Dunkl, I., & Brügl, A. (1998). Palinspastic reconstruction and topographic evolution of the Eastern Alps during late Tertiary tectonic extrusion. *Tectonophysics*, *297*, 1–15.
- Froitzheim, N., Conti, P., & van Daalen, M. (1997). Late Cretaceous, synorogenic, low-angle normal faulting along the Schlining fault (Switzerland, Italy, Austria) and its significance for the tectonics of the Eastern Alps. *Tectonophysics*, *280*, 267–293.
- Froitzheim, N., Plasienska, D., Schuster, R. (2008). Alpine tectonics of the Alps and Western Carpathians. In T. McCann (Ed.) *The Geology of Central Europe*, Vol 2, pp. 1141–1232. Geological Society London.
- Froitzheim, N., Schmid, S. M., & Conti, P. (1994). Repeated change from crustal shortening to orogen-parallel extension in the Austroalpine units of Graubünden. *Eclogae Geologicae Helveticae*, *87*, 559–612.
- Froitzheim, N., Weber, S., Nagel, T. J., Ibele, T., & Furrer, H. (2012). Late Cretaceous extension in the Northern Calcareous Alps (Schesaplana, rätkon, Switzerland and Austria). *International Journal of Earth Sciences (Geologische Rundschau)*, *101*, 1315–1329. doi:10.1007/s00531-011-0717-4.
- Fügenschuh, B., Mancktelow, N. S., & Seward, D. (2000). The Cretaceous to Neogene cooling and exhumation history of the Oetzal-Stubai basement complex, Eastern Alps: A structural and fission-track study. *Tectonics*, *19*(905–918), 2000.
- Galbraith, R. F., & Laslett, G. M. (1993). Statistical models for mixed fission track ages. *Nuclear Tracks and Radiation Measurements*, *21*, 459–470.
- Gleadow, A. J. W., Duddy, I. R., & Green, P. F. (1986). Fission track lengths in the apatite annealing zone and the interpretation of mixed ages. *Earth and Planetary Science Letters*, *78*, 245–254.
- Green, P. F., Duddy, I. R., Gleadow, A. J. W., Tingate, P. R., & Laslett, G. M. (1986). Thermal annealing of fission tracks in apatite 1. A qualitative description. *Chemical Geology*, *59*, 237–253.
- Hames, W., & Bowering, S. (1994). An empirical evaluation of the argon diffusion geometry in muscovite. *Earth and Planetary Science Letters*, *124*, 161–167.
- Handy, M. R., Franz, L., Heller, F., Janott, B., & Zurbriggen, R. (1999). Multistage accretion and exhumation of the continental crust (Ivrea crustal section, Italy and Switzerland). *Tectonics*, *18*(6), 1154–1177.
- Harrison, T. M., Célérier, J., Aikman, A. B., Hermann, J., & Heizler, M. T. (2009). Diffusion of ^{40}Ar in muscovite. *Geochimica et Cosmochimica Acta*, *73*(4), 1029–1051.
- Hirth, G., & Tullis, J. (1992). Dislocation creep regimes in quartz aggregates. *Journal of Structural Geology*, *14*, 145–159.
- Hoinkes, G., Höller, F., Rantitsch, G., Dachs, E., Höck, V., Neubauer, F., et al. (1999). Alpine metamorphism of the Eastern Alps. *Schweizerische Mineralogische und Petrographische Mitteilungen*, *79*, 155–181.
- Hoke, L. (1990). The Altkristallin of the Kreuzeck Mountains, SE Tauern Window, Eastern Alps; basement crust in a convergent plate boundary zone. *Jahrbuch der Geologischen Bundesanstalt Wien*, *133*, 5–87.
- Hurford, J., & Green, P. F. (1983). The zeta age calibration of fission-track dating. *Chemical Geology*, *41*, 285–312.
- Ketcham, R. A. (2005). Forward and inverse modelling of low-temperature thermochronometry data. In P. Reiners & T. A. Ehlers (Eds.), *Low-temperature thermochronology: Techniques, interpretations and applications. Reviews in Mineralogy & Geochemistry*, *58*, 275–314.
- Ketcham, R. A., Donelick, R. A., & Carlson, W. D. (1999). Variability of apatite fission-track annealing kinetics III: Extrapolation to geological time scales. *American Mineralogist*, *84*, 1235–1255.
- Kirschner, D., Cosc, M., Masson, H., & Hunziker, J. (1996). Staircase $^{40}\text{Ar}/^{39}\text{Ar}$ spectra of fine-grained white mica; timing and duration of deformation and empirical constraints on argon diffusion. *Geology*, *34*(8), 747–750.
- Kralik, M., Klima, K., & Riedmüller, G. (1987). Dating fault gouges. *Nature*, *327*(315–637), 317. doi:10.1038/327315a0.
- Kurz, W., & Fritz, H. (2003). Tectonometamorphic evolution of the Austroalpine Nappe Complex in the central Eastern Alps: Consequences for the Eo-alpine evolution of the Eastern Alps. *International Geology Review*, *45*, 1100–1127.
- Kurz, W., Wölfler, A., Rabitsch, R., & Genser, J. (2011). Polyphase movement on the Lavantal Fault Zone (Eastern Alps): Reconciling the evidence from different geochronological indicators. *Swiss Journal of Geosciences*, *104*(2), 323–343.
- Lambert, R. S. J. (1970). A potassium-argon study of the margin of the Tauernfenster at Döllach, Austria. *Eclogae Geologicae Helveticae*, *63*, 197–205.
- Lips, A. L. W., White, S. H., & Wijbrans, J. R. (1998). $^{40}\text{Ar}/^{39}\text{Ar}$ laserprobe direct dating of discrete deformational events: A continuous record of early Alpine tectonics in the Pelagonian Zone. *NE Aegean area, Greece, Tectonophysics*, *298*(133–653), 153.
- Liu, Y., Genser, J., Handler, R., Friedl, G., & Neubauer, F. (2001). $^{40}\text{Ar}/^{39}\text{Ar}$ muscovite ages from the Penninic-Austroalpine plate boundary, Eastern Alps. *Tectonics*, *20*, 526–547.
- Neubauer, F., Dallmeyer, R. D., Dunkl, I., & Schimik, D. (1995). Late Cretaceous exhumation of the metamorphic Gleinalm dome, Eastern Alps: Kinematics, cooling history and sedimentary response in a sinistral wrench corridor. *Tectonophysics*, *242*, 79–98.
- Neubauer, F., Genser, J., & Handler, R. (2000). The Eastern Alps: Result of a two-stage collision process. *Mitteilungen der Österreichischen Geologischen Gesellschaft*, *92*, 117–134.
- Neubauer, F., Hoinkes, G., Sassi, F. P., Handler, R., Höck, V., Koller, F., et al. (1999). Pre-Alpine metamorphism of the Eastern Alps. *Schweizerische Mineralogische und Petrographische Mitteilungen*, *79*, 41–62.
- Otsuki, K., Monzawa, N., & Nagase, T. (2003). Fluidization and melting of fault gouge during seismic slip: Identification in the Nojima fault zone and implications for focal earthquake mechanisms. *Journal of Geophysical Research*, *108*, 2003. doi:10.1029/2001JB001711.
- Oxburgh, E. R., Lambert, R. St. J., Baadsgaard, H., Simons, J. G. (1966). Potassium-argon age studies across the southeastern margin of the Tauern Window, the Eastern Alps. *Verhandlungen der Geologischen Bundesanstalt Wien*, 17–33.
- Roe, R. J. (1965). Description of crystallite orientation in polycrystalline materials. III. General solution to the pole figure inversion. *Journal of Applied Physics*, *36*, 2024–2031.
- Schmid, S. M., Fügenschuh, B., Kissling, B., & Schuster, R. (2004). Tectonic map of overall architecture of the Alpine orogen. *Eclogae Geologicae Helveticae*, *97*, 93–117.
- Schuster, R., Koller, F., Hoek, V., Hoinkes, G., & Bousquet, R. (2004). Explanatory notes to the map: Metamorphic structure of the Alps-metamorphic evolution of the Eastern Alps. *Mitteilungen der Österreichischen Mineralogischen Gesellschaft*, *149*, 175–199.

- Schuster, R., Kurz, W., Krenn, K., & Fritz, H. (2013). Introduction to the Geology of the Eastern Alps. *Berichte der Geologischen Bundesanstalt Wien*, 99, 121–133.
- Schuster, R., Scharbert, S., Abart, R., & Frank, W. (2001). Permo-Triassic extension and related HT/LP metamorphism in the Austroalpine: Southalpine realm. *Mitteilungen der Gesellschaft der Geologie- und Bergbaustudenten in Österreich*, 45, 111–141.
- Staufenberg, H. (1987). Apatite fission-track evidence for postmetamorphic uplift and cooling history of the eastern Tauern Window and the surrounding Austroalpine (Central Eastern Alps, Austria). *Jahrbuch der Geologischen Bundesanstalt Wien*, 13, 571–586.
- Stipp, M., Fügenschuh, B., Gromet, L. P., Stünitz, H., & Schmid, S. M. (2004). Contemporaneous plutonism and strike-slip faulting: A case study from the Tonale fault zone north of the Adamello pluton (Italian Alps). *Tectonics*. doi:10.1029/2003TC001515.
- Stipp, M., Stünitz, H., Heilbronner, R., & Schmid, S. M. (2002a). The eastern Tonale fault zone: A laboratory for crystal plastic deformation of quartz over a temperature range from 250 to 700 °C. *Journal of Structural Geology*, 24, 1861–1884.
- Stipp, M., Stünitz, H., Heilbronner, R., Schmid, S. M. (2002b). Dynamic recrystallization of quartz: Correlation between natural and experimental conditions. In De Meer, S., Drury, M. R., De Bresser, J. H. P., Pennock, G. M. (eds.), *Deformation mechanisms, rheology and tectonics: Current status and future perspectives*. Geological Society of London, *Special Publications*, 200, 171–190.
- Stipp, M., Tullis, J., & Behrens, H. (2006). Effect of water on the dislocation creep microstructure and flow stresses of quartz and implications for the recrystallized grain size piezometer. *Journal of Geophysical Research*. doi:10.1029/2005JB003852B04201.
- Stipp, M., Tullis, J., Scherwath, M., & Gehrman, J. J. (2010). A new perspective on paleopiezometry: Dynamically recrystallized grain size distributions indicate mechanism changes. *Geology*, 38(8), 759–762. doi:10.1130/G31162.1.
- Tagami, T. (2012). Thermochronological investigations of fault zones. *Tectonophysics*, 538–540, 67–85.
- Tagami, T., Hasabe, N., Kamohara, H., & Takemura, K. (2001). Thermal anomaly around the Nojima Fault as detected by fission-track analysis of Ogura 500 m borehole samples. *The Island Arc*, 10, 457–464.
- Tagami, T., & Murakami, M. (2007). Probing fault zone heterogeneity on the Nojima fault: Constraints from fission-track analysis of borehole samples. *Tectonophysics*, 443, 139–152.
- Toyoshima, T. (1990). Pseudotachylite from the Main Zone of the Hidaka metamorphic belt, Hokkaido, northern Japan. *Journal of Metamorphic Geology*, 8, 507–523.
- Wagner, G. A., & van den Haute, P. (1992). *Fission-Track Dating*. Stuttgart: Enke. 285 pp.
- Wagreich, M. (1995). Subduction tectonic erosion and Late Cretaceous subsidence along the northern Austroalpine margin (eastern Alps, Austria). *Tectonophysics*, 242, 63–78.
- Waters, D. J. (1976). Structural, metamorphic and geochronological studies in the south east Tauern Window. PhD Thesis, University of Oxford.
- Wenk, H. R. (1985). Measurements of pole figures. In H. R. Wenk (Ed.), *An introduction to modern texture analysis* (pp. 11–47). Orlando: Academic Press.
- Wölfler, A., Dekant, C., Danišák, M., Kurz, W., Dunkl, I., Putiš, M., & Frisch, W. (2008). Late stage differential exhumation of crustal blocks in the central Eastern Alps: Evidence from fission track and (U-Th)/He thermochronology. *Terra Nova*, 20, 378–384.
- Wölfler, A., Dekant, C., Frisch, W., Danišák, M., & Frank, W. (2015). Cretaceous to Miocene cooling of Austroalpine units southeast of the Tauern Window (Eastern Alps) constrained by multi-system thermochronometry. *Austrian Journal of Earth Sciences*, 108(1), 18–35.
- Wölfler, A., Kurz, W., Fritz, H., Stüwe, K. (2011). Lateral extrusion in the Eastern Alps revisited: Refining the model by thermochronological, sedimentary and seismic data. *Tectonics*, 30 TC4006. doi:10.1029/2010TC002782.
- Wölfler, A., Kurz, W., Wölfler, A., Danišák, M., & Rabitsch, R. (2010). Dating of fault zone activity by apatite fission track and apatite (U-Th)/He thermochronometry: A case study from the Lavanttal fault system (Eastern Alps). *Terra Nova*, 22, 274–282.
- Wölfler, A., Stüwe, K., Danišák, M., & Evans, N. J. (2012). Low temperature thermochronology in the Eastern Alps: Implications for structural and topographic evolution. *Tectonophysics*. doi:10.1016/j.tecto.2012.03016.
- Yamada, R., Matsuda, T., & Omura, K. (2007). Apatite and zircon fission-track dating from the Hirabayashi-NIED borehole, Nojima Fault, Japan: Evidence for anomalous heating in fracture zones. *Tectonophysics*, 443, 153–160.